





# Physical and numerical simulation of the production chain of fasteners manufactured of 32CrB4 steel control-cooled in the stelmor process to develop the multiphase microstructure

Michał Piwowarczyk<sup>1</sup>, Natalia Wolańska<sup>1</sup>, Marek Wilkus<sup>2</sup> , Maciej Pietrzyk<sup>2</sup> , Łukasz Rauch<sup>2</sup> , Roman Kuziak<sup>3</sup> , Valery Pidvysots'kyi<sup>3</sup> , Krzysztof Radwański<sup>3</sup>

<sup>1</sup> CMC Poland, ul. Piłsudskiego 82, 42-400 Zawiercie, Poland.

<sup>2</sup> AGH University of Krakow, Faculty of Metals Engineering and Industrial Computer Science, al. A. Mickiewicza 30, 30-059 Krakow, Poland.

<sup>3</sup> Łukasiewicz Research Network, Institute for Ferrous Metallurgy, ul. K. Miarki 12, 44-100 Gliwice, Poland.

## Abstract

The development of the concept of Thermomechanical Controlled Processing (TMCP) in the wire rod rolling mill of CMC Poland has opened up new opportunities for the production of fasteners without the application of heat treatment. The crucial effect of TMCP in the case of wire rod rolling is its capability of shaping fine austenite grain size following the last pass, typically below 20–25 μm in the wire rod cross-section. This is a prerequisite for obtaining the required cold workability level for the cold forming of fasteners, even if hard constituents (bainite, martensite) are present in the wire rod structure. In this paper, the physical simulation and numerical modelling capabilities were described for the design of cooling conditions in the Stelmor process and cold heading operation. The investigated material was conventional 32CrB4 grade used for the fasteners production with the application of heat treatment.

**Keywords:** wire rod, Stelmor process, multiphase steels, cold heading, numerical modelling

## 1. Introduction

The incentives for the investigation described in this paper are related to the development of the TMCP at CMC Poland for the production of the wire rod for cold heading applications. The CMC technology of TMCP rolling of wire rod with a diameter in the range of 8–25 mm is composed of the following stages:

- billet, 160 mm × 160 mm in cross-section, reheating to 1080–1100°C and holding during 0.5–2 hrs;

- rough rolling;
- intermediate rolling, when the final diameter of the wire rod is less than 14 mm;
- controlled cooling in the Stelmor line at a rate in the range of 0.5–10°C/s.

Application of the water boxes in the process of wire rod production allows for the band temperature to be obtained prior to the finishing mill in the range of 850–870°C, and following the finish rolling, the

\* Corresponding authors: [Natalia.Wolanska@cmc.com](mailto:Natalia.Wolanska@cmc.com)

ORCID ID's: 0000-0002-4700-6827 (M. Wilkus), 0000-0002-1473-4625 (M. Pietrzyk), 0000-0001-5366-743X (Ł. Rauch), 0000-0003-4965-5123 (R. Kuziak), 0000-0001-5199-1762 (V. Pidvysots'kyi)

© 2023 Authors. This is an open access publication, which can be used, distributed and reproduced in any medium according to the Creative Commons CC-BY 4.0 License requiring that the original work has been properly cited.

band temperature can be maintained in the range of 870–750°C before entering the Stelmor line. The lowest cooling rate of the wire rod cooled in the Stelmor line can be achieved by the application of the covers. In contrast, accelerated cooling can be accomplished by the application of fans. The application of the TMCP at the CMC Poland rolling mill enabled a very fine austenite grain size (below 20 μm) to be achieved in the wire rod after the final pass, which is a prerequisite for obtaining outstanding ductility and cold formability of any wire rod subject to controlled cooling in the Stelmor line. This feature of the TMCP wire rod motivated the investigation aimed at the development of multiphase microstructures in this semi-product with the intention of eliminating the heat treatment operation following the forming of the fasteners. Initially, low-carbon bainitic steels were recommended for this purpose by Kuziak et al. (2008). However, the quest for high-strength fasteners manufactured without the application of heat treatment motivated us to develop the semi-products of medium carbon steels composed of ferrite, bainite and martensite. The results obtained for grade 32CrB4 will be presented for the illustration example.

The investigation included three stages:

- developing the cooling schedules in the Stelmor line for obtaining predominantly ferritic-bainitic and martensitic microstructure in the wire rod using the phase transformation model described in the former investigation by Piwowarczyk et al. (2022);
- performing industrial experiments with designed cooling conditions followed by metallographic investigation with SEM;
- performing simulations of cold heading in Gleeble 3800 simulator using a dedicated die developed at Ł-IMZ.

## 2. Experimental material and methodology

The chemical composition of the industrial heat of 32CrB4 steel is given in Table 1. The continuously cast billets 160 mm × 160 mm in cross-section were hot rolled in the wire rod rolling mill of CMC Poland into ø10.5 mm wire rod followed by cooling in the Stelmor line according to the designed cooling variants. The billet reheating temperature prior to rolling was 1080°C, whilst the temperature of the wire rod at the lying head was around 850°C.

Samples of the wire rod were subject to investigation in the Gleeble 3800 thermal-mechanical simulator. First, the tests aimed at the rheological model development were performed. The uni-axial compression tests were performed on the samples having dimensions: ø7.7 × 9 mm, as schematically illustrated in Figure 1.

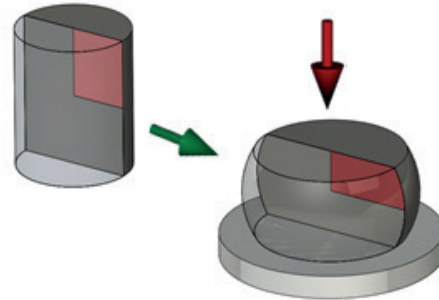


Fig. 1. Schematic illustration of the axi-symmetrical test

The tests were performed under constant strain rate conditions in the temperature range 20–100°C which allowed for accounting for the temperature increase during cold heading.

The physical simulation of cold heading was performed in the Gleeble 3800 thermal-mechanical simulator. The schematic picture of the homemade die is shown in Figure 2. The dimensions of the samples used in the cold heading simulations were: ø5 mm × 25 mm. The final shape of the sample was reached with one deformation conducted at an average strain rate in the range of 0.1–10 s<sup>-1</sup>.

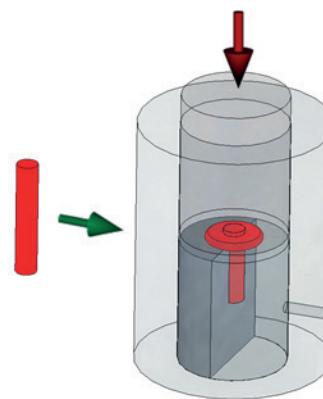


Fig. 2. A schematic picture of the die for the physical simulation of cold heading in the Gleeble 3800 simulator

Table 1. Chemical composition of the 32CrB4 steel [wt.%]

C	Mn	Si	P	S	Cr	Cu	Ni	Mo	Ti	B	N	Al
0.30	0.78	0.09	0.012	0.006	0.97	0.10	0.08	0.02	0.043	0.003	0.008	0.029

Metallographic samples were prepared by grinding and polishing with diamond paste. The investigation was carried out at a distance of approximately 0.2 mm from the spotted thermocouple. Microstructure observations were carried out with the optical and digital Olympus DSX500i microscope and with the high-resolution scanning electron microscopes (SEM) – JSM-7200F produced by Jeol and Inspect F by FEI. The samples were etched with 3% Nital. The quantitative measurements of the area fraction of the samples' microstructural constituents were performed with the Metilo program by J. Szala.

### 2.1. Developing cooling schedules for achieving multiphase structure of wire rod

The development of the phase transformations model for 32CrB4 steel was the subject of an earlier publication (Piwowarczyk et al., 2022). Therefore, only a brief summary of the developed model will be given below.

The general JMAK model (Avrami, 1939; Johnson & Mehl, 1939; Kolmogorov, 1937) was adapted to the condition of the cooling of wire rod after TMCP at the CMC Poland rolling line. The developed model is based on the Authors' numerical approach presented in (Pietrzyk & Kuziak, 2012). The changes which were introduced to the original JMAK equation are described below.

The classical JMAK equation is as follows:

$$X = 1 - \exp(-kt^n) \quad (1)$$

where:  $X$  – volume fraction of a new phase;  $t$  – time;  $k$ ,  $n$  – coefficients.

The upgrade of the JMAK model composed modification of equations describing the Avrami coefficient ( $k$ ) and incubation time. The incubation time was not introduced in the case of the ferritic transformation, and it was assumed that this transformation begins when 5% of ferrite is obtained. The Avrami coefficient for ferrite transformation ( $k_f$ ) is calculated as:

$$k_f = \frac{a_5}{D_\gamma^{a_{27}}} \exp \left[ - \left( \frac{|\Delta T|}{a_7} \right)^{a_8} \right] \quad (2)$$

where:

$$\Delta T = T - T_{nose} \quad T_{nose} = A_{e3} - \frac{400}{D_\gamma^{a_{27}}} + a_6 \quad (3)$$

The incubation time ( $\tau_p$ ) and Avrami coefficient ( $k_p$ ) for pearlitic transformation as well as incubation time ( $\tau_b$ )

and Avrami coefficient ( $k_b$ ) for bainitic transformation, are calculated as follows:

$$\tau_p = \frac{a_9 D_\gamma^{a_{28}}}{(A_{c1} - T)^{a_{11}}} \exp \left[ \frac{a_{10}}{R(T + 273)} \right] \quad (4)$$

$$k_p = \frac{a_{15}}{D_\gamma^{a_{14}}} \exp \left[ - \left( \frac{|T - a_{12}|}{a_{13}} \right)^2 \right] \quad (5)$$

$$\tau_b = \frac{a_{17} D_\gamma^{a_{30}}}{(a_{20} - T)^{a_{19}}} \exp \left[ \frac{a_{18}}{R(T + 273)} \right] \quad (6)$$

$$k_b = \frac{a_{23}}{D_\gamma^{a_{29}}} \exp \left[ - \left( \frac{|T - a_{21}|}{a_{22}} \right)^2 \right] \quad (7)$$

The introduction of the modified Gauss function in the  $k(T)$  relation was the main change comparing to (Pietrzyk & Kuziak, 2012). This function allowed reproduction of the C shape of the isothermal transformation curve. The exponential functions, which were originally used in (Pietrzyk & Kuziak, 2012) gave a continuous increase in the rate of transformation with the decreasing temperature, which is not physical. The remaining equations in the model include:

– martensite start temperature:

$$M_s = a_{25} - a_{26} c_\gamma \quad (8)$$

– martensite volume fraction (Koistinen & Marburger, 1959):

$$F_m = (1 - F_f - F_p - F_b) \left\{ 1 - \exp[-0.011(M_s - T)] \right\} \quad (9)$$

where:  $F_f$ ,  $F_p$ ,  $F_b$ ,  $F_m$  – volume fractions of ferrite, pearlite, bainite and martensite.

Coefficient  $a_{20}$  in the Equation (6) represents the bainite start temperature. During the simulation of the ferritic transformation, the average carbon concentration in the austenite is calculated as:

$$c_\gamma = \frac{c_0 - F_f c_\alpha}{1 - F_f} \quad (10)$$

where  $c_0$  – carbon content in steel.

In the developed model, the equilibrium content of phases is calculated with the ThermoCalc computer program (Andersson et al., 2002).

## 3. Cooling experiments in the Stelmor line

The industrial trials include rolling of 10.5 mm in diameter wire rod of 32CrB4 steel. Three variants of

cooling were designed for the cooling experiments in the Stelmor line:

- slow cooling resulting in the formation of ferrite – pearlite microstructure – cooling variant referred to as W280;
- two-stage cooling aimed at the development of the multiphase microstructure composed of ferrite (~30%) and predominantly bainite – cooling variant referred to W395;
- two-stage cooling aimed at the development of the multiphase microstructure composed of ferrite (~30%) and predominantly martensite – cooling variant referred to as W440.

The phase transformation model was used to design the cooling curves to meet these assumptions regarding the microstructure constituents, and the results in the form of cooling curves and predicted volume fractions of ferrite, pearlite, bainite and martensite at the end of cooling are presented in Figure 3.

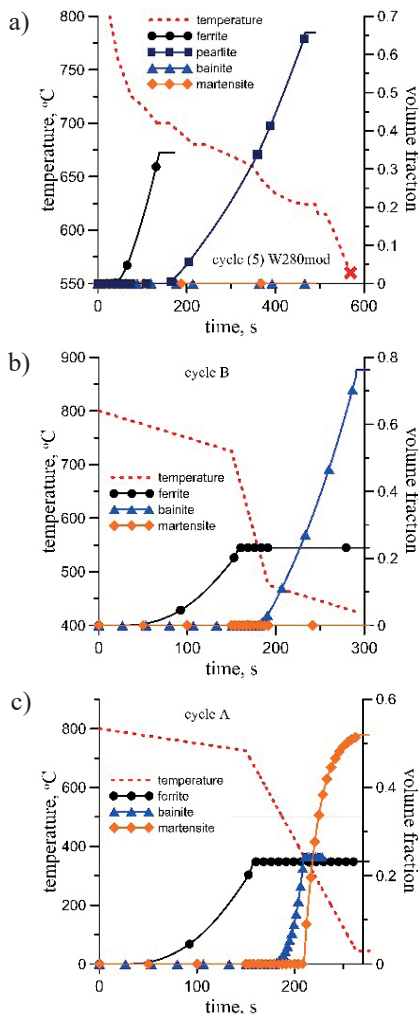


**Fig. 3.** Developed cooling curves for cooling of  $\varnothing 10$  mm wire rod of 32CrB4 steel in the Stelmor line: a) variant W280; b) variant W395; c) variant W440

The obtained cooling curves during the industrial trials measured with an infrared camera are presented in Figure 4. The cooling conditions in the Stelmor line were adjusted by applying different configurations and settings of the air fans.

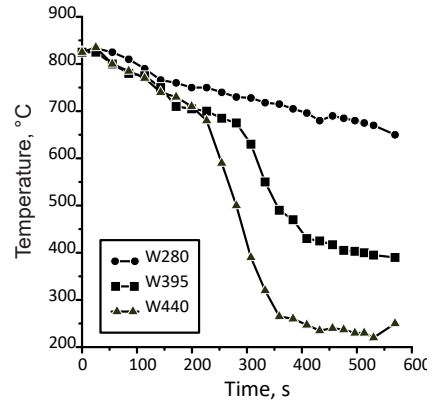


**Fig. 4.** Measured variations of the surface temperature as a function of time in the performed industrial trials in the CMC Poland Stelmor. Measurements were performed at the low-density region of the wire loops

The measured cooling curves are very close to the designed ones. Furthermore, the obtained microstructure and area fractions of microstructural constituents are close to the predicted values (Fig. 5, Tab. 2). In the sample subject to the W395 variant, both types of bainite microstructure, namely lower and upper, are present. The microstructure of this sample also contains martensite. The mechanical properties of the wire rod after different variants of cooling are given in Table 3.

**Table 2.** Measured fractions of microstructure constituents in the  $\varnothing 10.5$  mm wire rod of 32CrB4 steel obtained during industrial trials

Variant	Ferrite	Pearlite	Bainite	Martensite
W280	0.40	0.60	–	–
W395	0.38	0.03	0.48	0.11
W440	0.25	0.08	0.12	0.55

**Table 3.** Mechanical properties of the  $\varnothing 10.5$  mm wire rod of 32CrB4 steel obtained during industrial trials

Variant	$R_{p0.2}$ [MPa]	$R_m$ [MPa]	$A_5$ [%]	Z
W280	398	666	30.5	64.5
W395	461	723	24.6	56.5
W440	452	786	22.8	52.1

The results of the mechanical properties measurement indicate that the Ultimate Tensile Strength (UTS) of the wire rod subject to different cooling variants is dependent on the fraction of microstructural constituents.

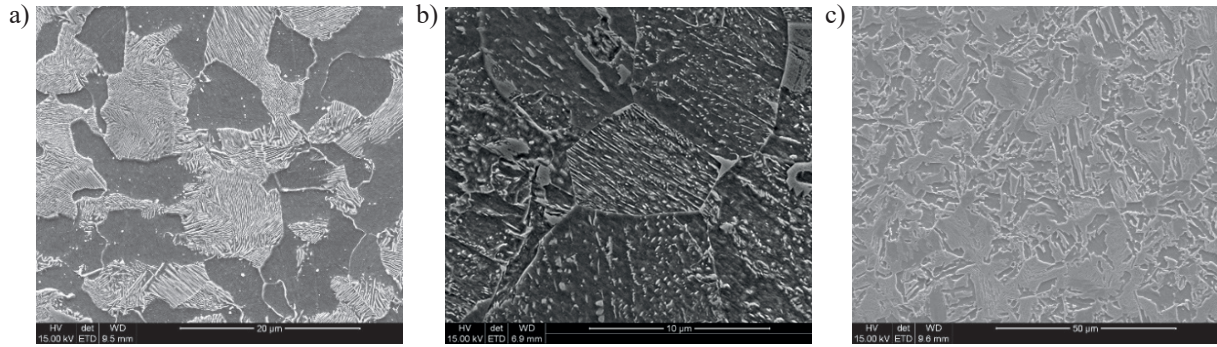


**Fig. 5.** Microstructure of the wire rod  $\varnothing 10$  mm of 32CrB4 steel in the Stelmor line: a) variant W280; b) variant W395; c) variant W440

The highest value of UTS is obtained for the wire rod containing martensite, however, in this case, the values of Elongation to Fracture and Reduction of Area are the lowest of all the cooling variants.

## 4. Physical and numerical simulation of cold heading

### Physical simulation

Physical simulations of cold heading were performed with the die shown in Figure 2 installed in Gleeble 3800 simulator. The rod samples  $\varnothing 5$  mm  $\times$  25 mm were deformed at an average strain rate of  $0.1 \text{ s}^{-1}$ ,  $1 \text{ s}^{-1}$  and  $10 \text{ s}^{-1}$ . The macrostructure of the deformed samples in the plane of symmetry is shown in Figure 6 after 5% Nital etching.

The dark grey areas in the cross section coincide with the zones of localised plastic flow. The head of the samples of W280 and W395 variants show no occurrence of cracks. In contrast, in the case of the cold-headed sample of variant W440, a crack developed on the head perimeter (shown with a white arrow in Figure 6c).

The microstructure of the samples (marked with 1 and 2) is shown in Figures 7–9. It can be seen that both ferrite and second hard constituents are subject to intense plastic flow causing their elongation, however the strain distribution in the ferrite is more homogeneous than in the pearlite, bainite and martensite. This may be caused by the differences in the strength and morphological features of these constituents. The sample of the W440 variant exhibits the most pronounced plastic flow localisation (Fig. 9). Samples of this variant are more prone to cracking, specifically at the bainite/martensite interface (Fig. 10).



**Fig. 6.** Macrostructure of the cold-headed samples of wire rod of 32CrB4 steel after the following variants of cooling: a) variant W280; b) variant W395; c) variant W440. The average strain rate was  $10 \text{ s}^{-1}$

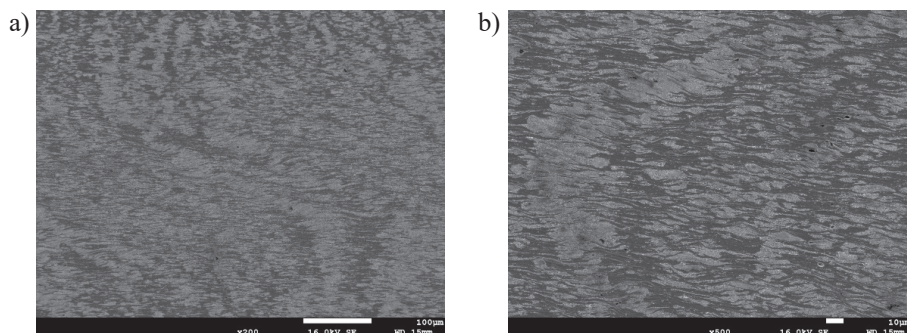


**Fig. 7.** Microstructure of the sample W280 after cold heading at an average strain rate of  $10 \text{ s}^{-1}$ : a) point 1; b) point 2

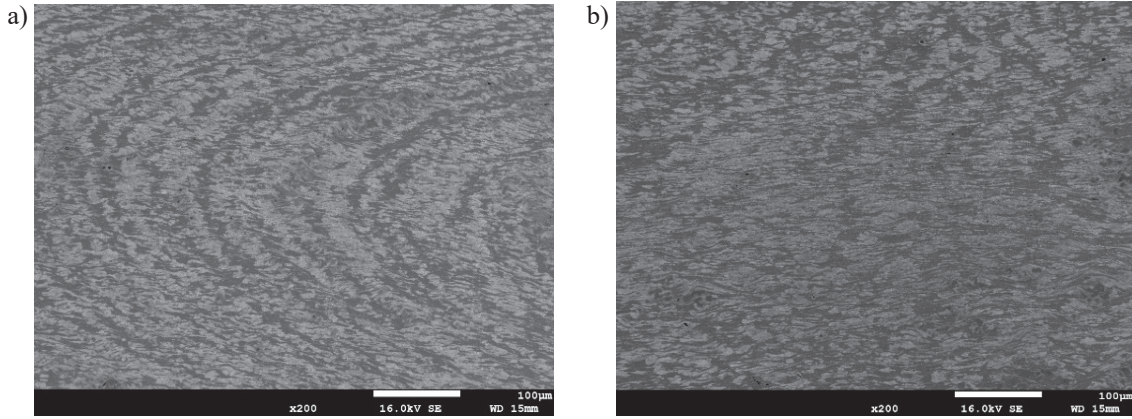


**Fig. 8.** Microstructure of the sample W395 after cold heading at an average strain rate of  $10 \text{ s}^{-1}$ : a) point 1; b) point 2

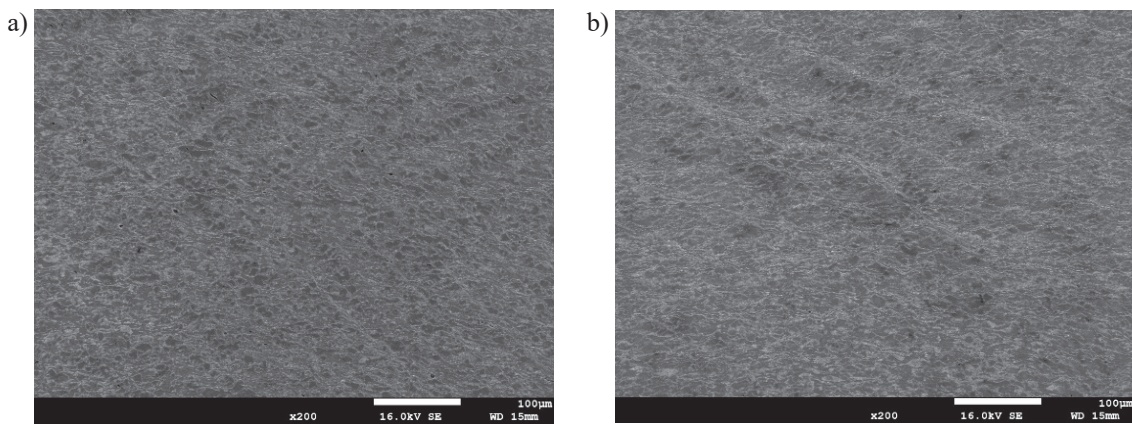


**Fig. 9.** Microstructure of the sample W440 after cold heading with an average strain rate of  $10 \text{ s}^{-1}$ : a) point 1; b) point 2

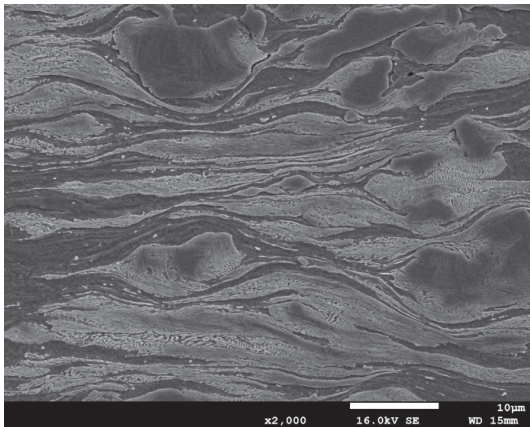


**Fig. 10.** Microstructure of the sample W440 after cold heading with an average strain rate of  $10 \text{ s}^{-1}$  at the perimeter area. The arrow marks the occurrence of a crack at the bainite/martensite interface

### Numerical modelling

The numerical simulation of head forming was made using FORGE FE software. Models for the considered materials have been implemented as own Hensel–Spittel

equations (Hensel & Spittel, 1979) describing material behavior:

$$\sigma = K\varepsilon^m \exp(-q\varepsilon) \dot{\varepsilon}^n \exp(-\beta T) \quad (11)$$

where:  $\sigma$  – flow stress;  $\varepsilon$  – strain;  $\dot{\varepsilon}$  – strain rate;  $T$  – temperature [ $^{\circ}\text{C}$ ];  $K$ ,  $m$ ,  $q$ ,  $n$ ,  $\beta$  – coefficients, which were determined using inverse analysis for the uniaxial compression tests.

The constitutive law in the software is based on the Norton–Hoff equation (Chenot & Bellet, 1992). A typical cold-forming setup has been used. The friction coefficient was implemented using the Coulomb formula with the threshold and with the software’s pre-defined values. The tool kinematics parameters have been identified from the recorded die displacement as a function of time. The normalized Latham–Cockcroft (LC) criterion was used to evaluate the local tendency to cracks. The isotropic damage evolution equation is (Cockcroft & Latham, 1968):

$$\int_0^{\varepsilon} \frac{\sigma_1}{\sigma} d\varepsilon \geq C \quad (12)$$

where  $\sigma_1$  – the largest principal stress.

According to the LC criterion, the fracture occurs when an integral in Equation (12) exceeds a certain critical value  $C$ . The LC criterion was implemented in the FE software using the user's subroutine. The largest principal stress, the equivalent stress (equal to flow stress) and the strain were calculated iteratively.

In processes like fastener forging, a significant difference in strain values is present in the workpiece. Such differences require remeshing during computation, which is a time and resource consuming part of the whole workflow. To obtain results in a reasonable time, a field-based adaptive remeshing has been used for the final calculations. Typical tetrahedron elements have been used. The calculations have been performed using 3D solver with a 90-degree revolved part. The symmetry boundary conditions were applied to the symmetry planes.

The identification of the coefficients in the Equation (11) was performed by the inverse analysis of the plastometric test results. The problem of parameter identification is defined as the inverse problem. The commonly used method to solve such a task, where the direct problem is formulated with a linear differential equation, is to transform it into the optimization task with the goal function defined as the distance between calculated and measured data in the norm defined in the functional value space. The minimum of the goal function is the solution of the inverse problem. The inverse algorithm developed by Szeliga et al. (2006) was used. This algorithm consists of three steps:

1. Performing physical experiments and collecting the obtained data.
2. Performing simulations of the experiments at constant physical conditions (temperatures, strain rates) and elaborating the collected data.
3. Running optimization procedure to minimize the difference between measured and calculated data with respect to the parameters of the material flow stress model.

For the optimization task, the goal function is defined as the mean square root error between measured and calculated loads recorded during the compression process:

$$\Phi(\mathbf{x}) = \frac{1}{Nt} \sum_{i=1}^{Nt} \left[ \frac{1}{Ns} \sum_{j=1}^{Ns} \left( \frac{F_c^{ij} - F_m^{ij}}{F_m^{ij}} \right)^2 \right] \quad (13)$$

where:  $\mathbf{x}$  – vector of the material parameters ( $A$ ,  $m$ ,  $q$ ,  $n$ ,  $\beta$ ) in the flow stress equation;  $F_m$ ,  $F_c$  – measured and calculated loads in the compression test;  $Ns$  – number of sampling points in one test;  $Nt$  – number of tests (it accounts for all tests performed at various temperatures and various strain rates).

Analysis of the results of the compression tests has shown that the effect of the strain rate and the temperature is small. The measured compression forces for the temperature 100°C are shown in Figure 11. Coefficients determined using inverse analysis are given in Table 4.

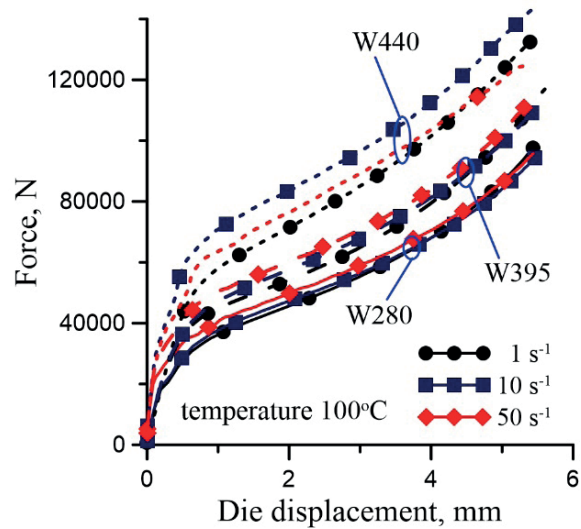


Fig. 11. Measured forces vs. die displacement for the temperature 100°C

Table 4. Coefficients in the Equation (11) for the investigated samples

Sample	$A$	$m$	$q$	$n$	$\beta$
W280	1404.7	0.266	0.497	0.0165	0.00085
W378	2234.9	0.272	0.625	0.008	0.00069
W395	1528.1	0.217	0.442	0.008	0.000423

The results of the FE simulations are presented in Figure 12 for the sample W280, in Figure 13 for the sample W395 and in Figure 14 for the sample W440. Since the effect of the process parameters was small, the results for the temperature 20°C and the strain rate 10 s<sup>-1</sup> only are presented. It is seen that distributions of strains are similar for the three samples with the largest values concentrated in the connection between the head and the core. In contrast, the material has an influence on the effective stress and on the LC criterion. The largest values of the stress and the LC were obtained for the ferritic-martensitic microstructure (W440), smaller for the ferritic-bainitic microstructure (W395) and the smallest for the ferritic-pearlitic microstructure (W280). As expected, the largest values of the LC criterion were obtained at the perimeter of the head on the sample.

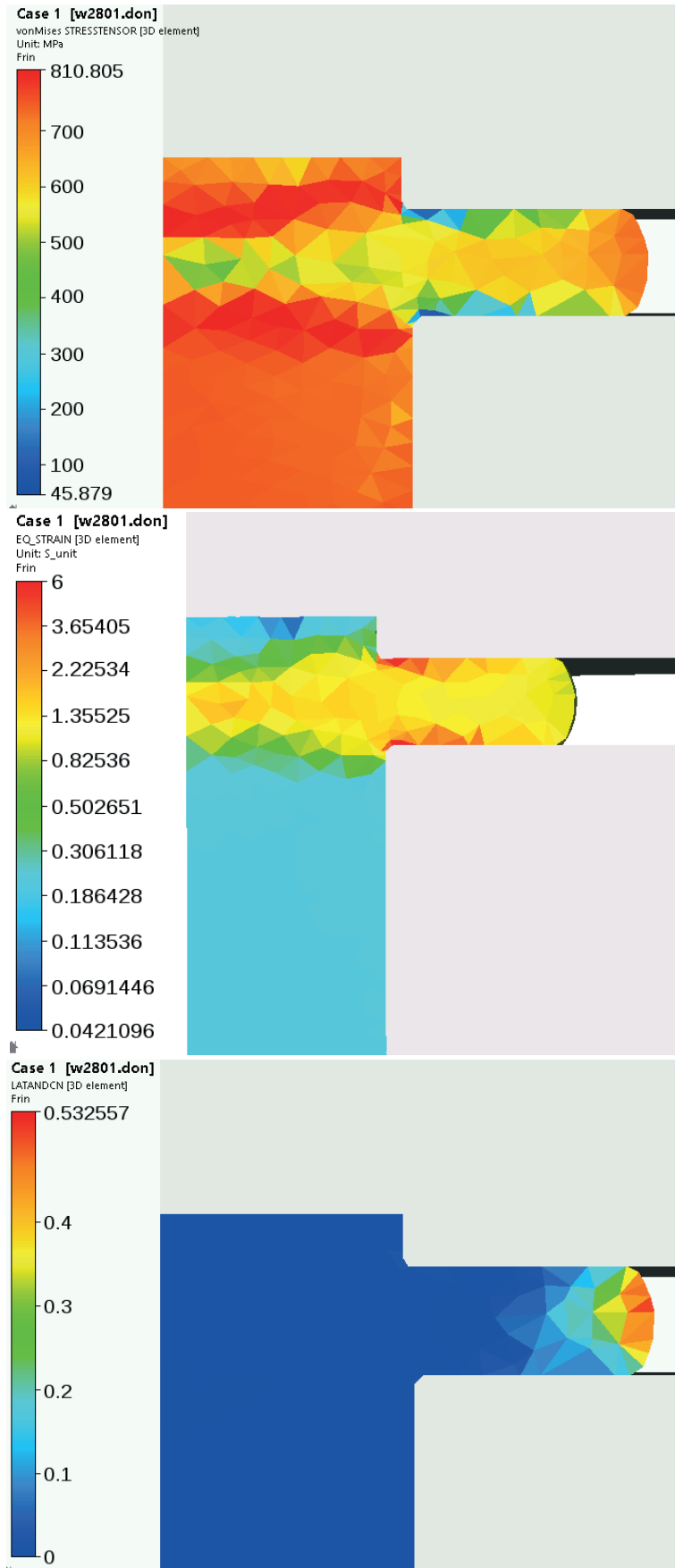


Fig. 12. Calculated distributions of the effective stress, the effective strain and the LC criterion for the sample W280



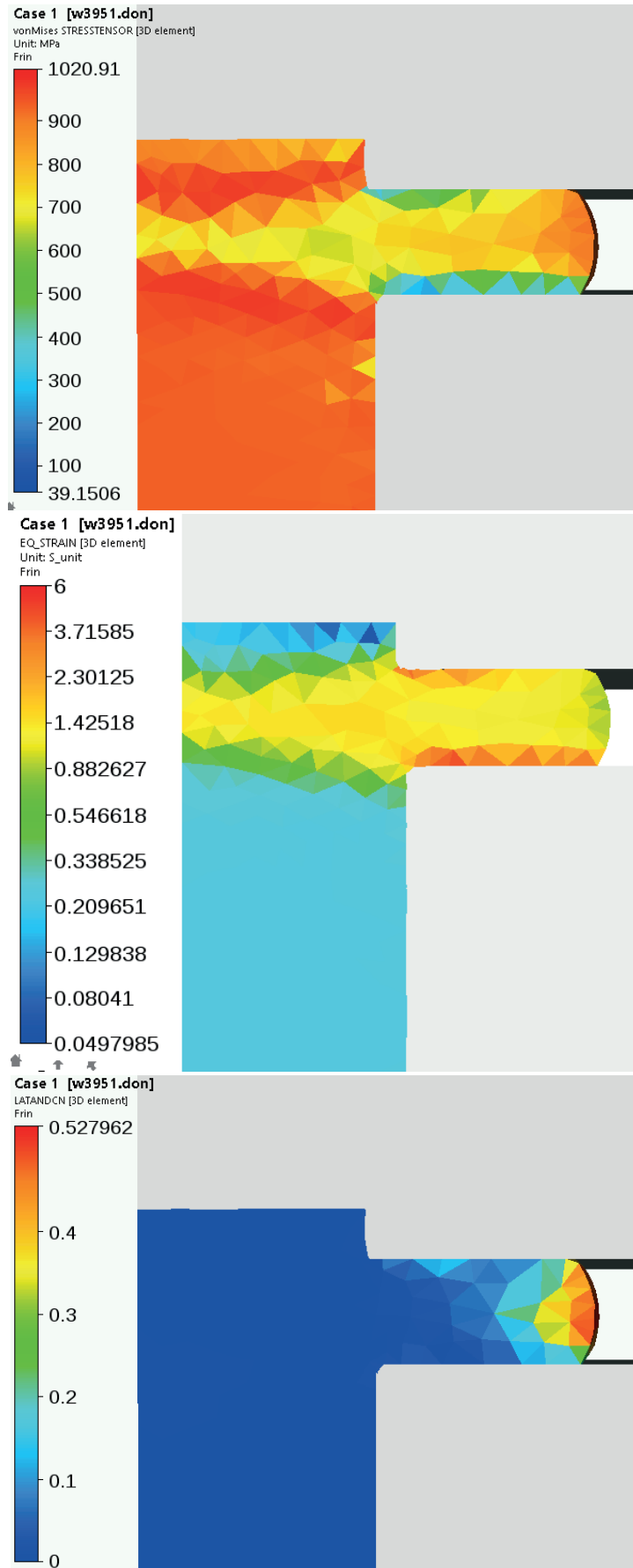


Fig. 13. Calculated distributions of the effective stress, the effective strain and the LC criterion for the sample W395

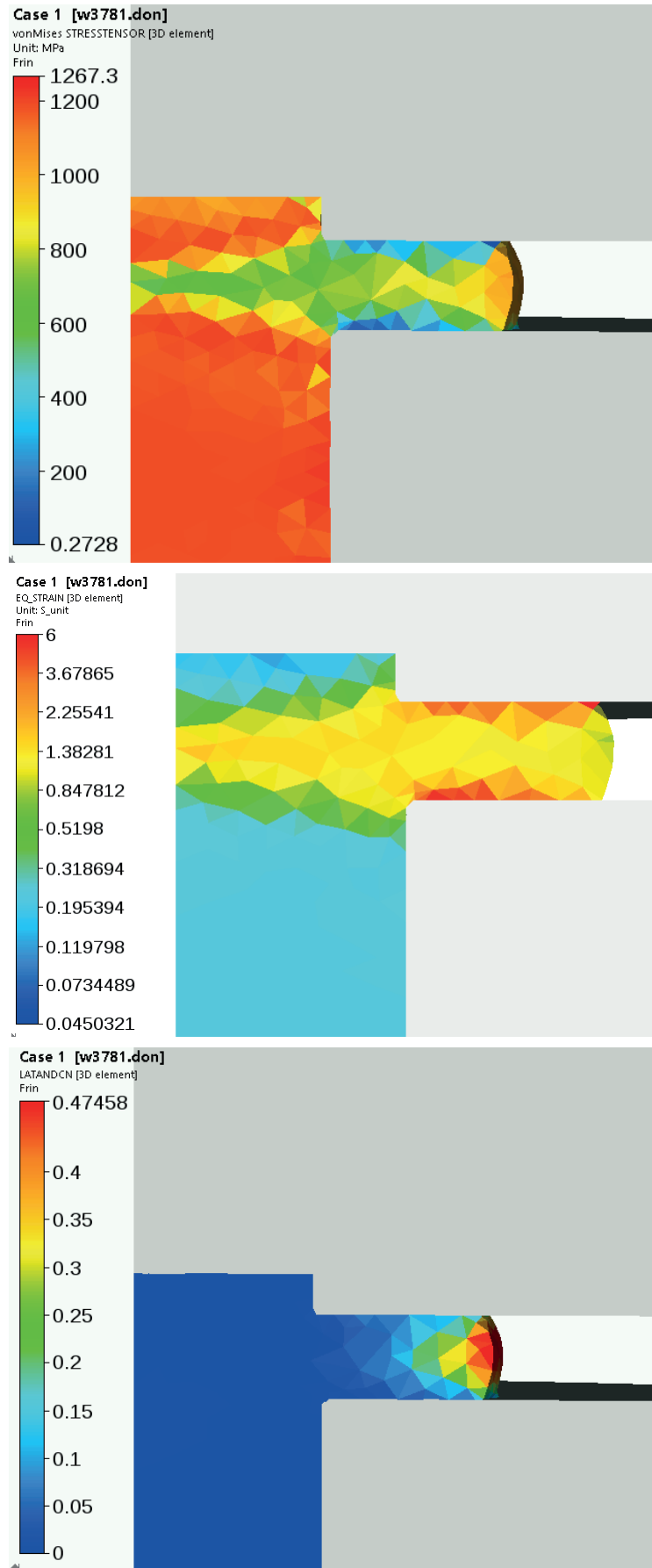


Fig. 14. Calculated distributions of the effective stress, the effective strain and the LC criterion for the sample W440

## 5. Discussion

The most commonly used microstructure for the cold heading is obtained by the application spheroidizing annealing. This process transforms the original ferrite-pearlite microstructure into one composed of a continuous ferrite matrix with spheroidal carbides (cementite). This microstructure provides the required degree of technological plasticity for severe cold deformation.

Since spheroidizing annealing is an energy-consuming and environmentally harmful technology, metallurgists have focused over the last two decades on the development of steel grades enabling obtaining the required properties of fasteners without the application of heat treatment operations (Fig. 15).

In the Coheadbain project, a new generation of low-carbon bainitic steels was developed which was capable of developing the required properties of

8.8 class of fasteners without the application of heat treatment (Kuziak et al., 2008). The favourable microstructure of the wire rod of the bainitic steels developed in this project was the granular bainite.

The investigation presented in this paper has shown that the wire rod composed of the mixture of ferrite and upper and lower bainite can be used successfully for the production of fasteners without the application of heat treatment operations. The reason for the behaviour of upper and lower bainite is probably related to the morphology of iron carbide particles that are very small. The size and shape of second-phase particles affect the characteristics of fracture. According to Fisher & Gurland (1981), decreasing the dimensions of the second phase will increase the critical stress required to cause particle cracking and improve cold headability (Fig. 16).

Furthermore, the bainitic structure of the wire rod enables the use of two variants of fastener production, namely with and without final heat treatment.

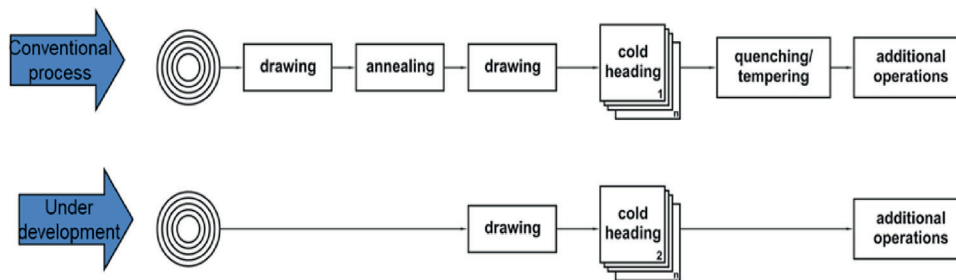


Fig. 15. Modification of the classical technology of the production of fasteners

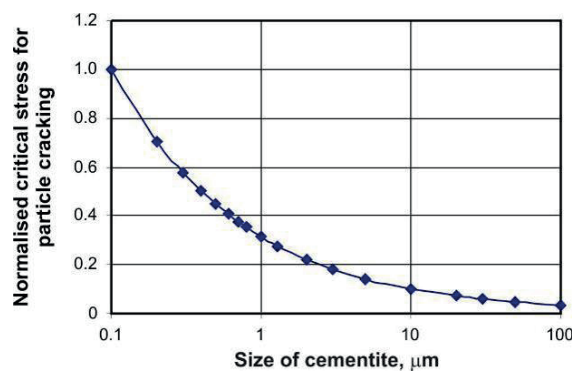


Fig. 16. The effect of particle size on the critical stress for particle cracking (Fisher & Gurland, 1981)

## 6. Conclusions

1. The results obtained in the presented investigations confirmed the good predictive capability of the modified phase transformations model to design the cooling conditions in the Stelmor line for the development of multiphase structure of conventional steel grades used for the fasteners production.
2. Both ferrite pearlite and ferrite bainite microstructure of the wire rod of 32CrB4 steel enables the production of fasteners without the application of heat treatment operations.
3. The microstructure of the wire rod composed of ferrite and bainite mixture exhibits higher resistance to cold heading as compared to the ferrite pearlite microstructure. This can lead to a lowering usage time of forming tools.

4. It was found that the development of cracking in the wire rod microstructure containing predominantly ferrite and bainite was connected to the occurrence of a small island of bainite. The cracks formed preferably at the interface between bainite and martensite.

## Acknowledgements

This paper and research was created with the support financed by European Funds – Smart Growth (European Union, European Regional Development Fund) grant number POIR.01.02.00-00-0159/16.

---

## References

- Andersson, J.O., Helander, T., Höglund, L., Shi, P.F. & Sundman, B. (2002). Thermo-Calc and DICTRA, computational tools for materials science. *Calphad*, 26(2), 273–312. [https://doi.org/10.1016/S0364-5916\(02\)00037-8](https://doi.org/10.1016/S0364-5916(02)00037-8).
- Avrami, M. (1939). Kinetics of phase change. I. General theory. *The Journal of Chemical Physics*, 7, 1103–1112. <https://doi.org/10.1063/1.1750380>.
- Chenot, J.-L. & Bellet, M. (1992). The viscoplastic approach for the finite-element modelling of metal forming processes. In P. Hartley, I. Pillinger, C. Sturges (Eds.), *Numerical modelling of material deformation processes. Research, Development and Applications* (pp. 179–224). Springer London. [https://doi.org/10.1007/978-1-4471-1745-2\\_8](https://doi.org/10.1007/978-1-4471-1745-2_8).
- Cockroft, M.G. & Latham, D.J. (1968). Ductility and the workability of metals. *Journal of the Institute of Metals*, 96, 33–39.
- Fisher, J.R. & Gurland, J. (1981). Void nucleation in spheroidized carbon steels. *Metal Science*, 15(5), 18.
- Hensel, A. & Spittel, T. (1979). *Kraft- und Arbeitsbedarf bildsamer Formgebungsverfahren*. VEB Deutscher Verlag für Grundstoffindustrie.
- Johnson, W.A. & Mehl, R.F. (1939). Reaction kinetics in processes of nucleation and growth. *Transactions AIME*, 135, 416–442.
- Koistinen, D.P. & Marburger, R.E. (1959). A general equation prescribing the extent of the austenite-martensite transformation in pure iron-carbon alloys and plain carbon steels. *Acta Metallurgica*, 7, 59–69. [https://doi.org/10.1016/0001-6160\(59\)90170-1](https://doi.org/10.1016/0001-6160(59)90170-1).
- Kolmogorov, A. (1937). К статистической теории кристаллизации металлов. *Izvestiya Akademii Nauk SSSR*, 1(3), 355–359 [К статистической теории кристаллизации металлов. *Известия Академии Наук СССР*, 1(3), 355–359].
- Kuziak, R., Zajac, S., Kawalla, R., Waengler, S., Stercken, K., Jakobczak, R., Urlau, R. & Hasler, R. (2008). *Cold Heading Quality Low-Carbon Ultra-High-Strength Bainitic Steels*. Final Report. RFCS Project No. RFSR-CT-2005-00031.
- Pietrzyk, M. & Kuziak, R. (2012). Modelling phase transformations in steel. In J. Lin, D. Balint, M. Pietrzyk (Eds.), *Microstructure Evolution in Metal Forming Processes* (pp. 145–179). Woodhead Publishing.
- Piwoarczyk, M., Wolanska, N., Pietrzyk, M., Rauch, Ł., Kuziak, R. & Zalecki, W. (2022). Phase transformation model for adjusting the cooling conditions in Stelmor process to obtain the targeted structure of thermomechanically rolled wire rod used for fastener production. *Metallurgical Research Technology*, 119(5), 517. <https://doi.org/10.1051/metal/2022071>.
- Szala, J. *Metilo* (version 12.01a). Katowice Silesian University of Technology, Institute of Materials Science.
- Szeliga, D., Gawad, J. & Pietrzyk, M. (2006). Inverse analysis for identification of rheological and friction models in metal forming. *Computer Methods in Applied Mechanics and Engineering*, 195, 6778–6798. <https://doi.org/10.1016/j.cma.2005.03.015>.